Research Square

Preprints are preliminary reports that have not undergone peer review.
They should not be considered conclusive, used to inform clinical practice,
or referenced by the media as validated information.

CoFe2O4@SiO2/HKUST-1, A Novel Three-Metallic Magnetic Metal-Organic Framework: Synthesis, Methylene Blue Removal, the Study of Adsorption Isotherms and Kinetic Models

Tahoura Saemian
Azarbaijan Shahid Madani University
Moayad Hossaini Sadr (hosainis@yahoo.com)
Azarbaijan Shahid Madani University https://orcid.org/0000-0003-0119-7709
Mehrnaz Gharagozlou
Institute for Color Science and Technology
Behzad Soltani
Azarbaijan Shahid Madani University

Research Article

Keywords: CoFe2O4@SiO2/HKUST-1, magnetic metal-organic framework (MMOF), self-assembly method, methylene blue, adsorption isotherms and kinetic models

Posted Date: July 29th, 2021

DOI: https://doi.org/10.21203/rs.3.rs-749264/v1

License: This work is licensed under a Creative Commons Attribution 4.0 International License.
Read Full License

$CoFe_2O_4$@SiO_2/HKUST-1, a novel three-metallic magnetic metal-organic framework: synthesis, methylene blue removal, the study of adsorption isotherms and kinetic models

Tahoura Saemian[a, b], Moayad Hossaini Sadr[a,*], Mehrnaz Gharagozlou[b], Behzad Soltani[a]

[a] Department of Chemistry, Faculty of Science, Azarbaijan Shahid Madani University, Tabriz, Iran

[b] Department of Nanomaterials and Nanocoatings, Institute for Color Science and Technology, Tehran, Iran

Abstract

* Corresponding Author: Moayad Hossaini Sadr, Department of Chemistry, Azarbaijan Shahid Madani University, P. O. Box 53714-161, Tabriz, Iran.

https://orcid.org/0000-0003-0119-7709

, Tel, Fax: +984134327526hosainis@yahoo.com

$CoFe_2O_4@SiO_2$/HKUST-1 as a novel three-metallic magnetic metal-organic framework (MMOF) has been favorably synthesized via a simple self-assembly method. For this purpose, $CoFe_2O_4@SiO_2$ was functionalized by Glutaric anhydride and 3-(triethoxysilyl)propylamine and then HKUST-1 was synthesized on the surface of $CoFe_2O_4@SiO_2$. Powder X-ray diffractometry (XRD), Fourier transform infrared (FTIR), scanning electron microscopy (SEM) and transmission electron microscopy (TEM), Brunauer-Emmett-Teller (BET), vibrating sample magnetometer (VSM), and simulated thermal analyzer (STA) were utilized to characterize the as-prepared samples. The methylene blue (MB) removal efficiency of $CoFe_2O_4@SiO_2$/HKUST-1 has been set by examining factors such as the effect of pH, concentration of dye, amount of adsorbent, and components of a compound. Up to 100 percent dye removal in short reaction times and water media was reached in alkaline pH, by increasing the dose of adsorbent and in the presence of $CoFe_2O_4@SiO_2$ and $CoFe_2O_4@SiO_2$/HKUST-1 compounds. Freundlich adsorption isotherm that uses to describe the ongoing adsorption was found to be best fitted for the adsorption process.

Based on pseudo-first-order, pseudo-second-order, and intraparticle diffusion kinetic equations, the pseudo-second-order kinetic model with rate constant (k^2) 4 $x10^{-3}$ g/mg.min is best fitted for adsorption methylene blue, indicating that removal of dye takes place dominantly through the chemisorption process.

Keywords: $CoFe_2O_4$@SiO_2/HKUST-1, magnetic metal-organic framework (MMOF), self-assembly method, methylene blue, adsorption isotherms and kinetic models

1. Introduction

Metal-organic frameworks, MOFs, as an emerging class of organic-inorganic hybrid crystalline porous materials due to the diverse combination of coordinating metal ion centers and organic linkers have versatile structures and applications [1-2]. MOFs have received considerable attention in the last decade because of the exciting features like large specific surface area, adjustable pore volume, tunable surface, thermal stability, modifiable pores, and enriched host-guest chemical properties. These properties can be beneficial to solve environmental issues such as toxic and pollutant gas capture, storage, and separation [3–7].

Among thousands of known MOFs, the HKUST-1 (Hong Kong University of Science and Technology), because of reasonable stability in the aquatic environment, is one of the rare MOFs used in aqueous applications, including removing heavy metals and organic contaminants [8–12].

Since MOFs may collapse in aqueous environments, their recycling from the solution is problematic to resolve this issue; using other components can improve the performance of MOFs in different applications. Magnetic metal-organic

framework composites (MMOF) are one that compound, which due to their inheriting the superiorities of magnetic nanoparticles and MOFs, provide a synergistic effect and expanded specific novel functionalities including drug delivery and imaging, environmental remediation and separation, and especially water purification [13–16].

Cobalt ferrite ($CoFe_2O_4$) is one of the most appealing magnetic materials to make magnetic metal-organic frameworks due to its desired magnetic, mechanical and chemical properties. On the other hand, the silica matrix for ferrite nanoparticle dispersion is too important to improve magnetic properties, nanoparticle aggregation control, stability, and disperse in aqueous [17,18]. Several studies have reported applications of the same magnetic system in wastewater purification. For instance, L. Huang and coworkers reported Fe_3O_4@SiO_2@HKUST-1 magnetic core-shell composite to enhanced removal of Hg^{2+} from water [19], Ruiqi Zhang too reported magG@SiO_2@ZIF-8 [20], and similar magnetic composites based on the magnetic nanoparticles coated with SiO_2 and MOF, Fe_3O_4@SiO_2@MOF/TiO_2 [21], Fe_3O_4@SiO_2@Zn-TDPAT [22] and Fe_3O_4@SiO_2@Zr-MOF [23] were successfully synthesized in order to remove of organic contaminants from the environment.

United Nations General Assembly in 2015 approved the 17 Sustainable Development Goals, SDGs, as the “blueprint to achieve a better and more

sustainable future for all" [24] and the 7 of the SDGs directly or indirectly emphasize environmental protection. Fortunately, a good deal of research is taking place as well in order to remove pollutants from the environment and protection of water, soil, air and the atmosphere [25–27].

Among water pollutants, textile dyeing and finishing procedures are the primary sources of pollution and cause a high amount of dye in wastewater [27]. Therefore, removing dyes from water is imperative due to its harmful effects like toxicity, carcinogenesis, suppressing photosynthetic activities, causing allergic reactions, mutagenesis, and inhibiting the growth of aquatic biota [28]. Methylene blue (MB) as a well-known cationic dye with diverse industrial applications was selected to serve as a contaminant model [29,30].

In this work, a novel magnetic $CoFe_2O_4$@SiO_2/HKUST-1 nanocomposite was prepared via an in situ self-assembly method. This method includes modifying pre-synthesized magnetic $CoFe_2O_4$@SiO_2 particles and inducing them to copper nitrate and benzene-1,3,5-tricarboxylic acid (H_3BTC) solution to self-assembly fabricate $CoFe_2O_4$@SiO_2/HKUST-1 magnetic metal-organic framework. The newly synthesized compound needs to identify to understand it better and then apply it to remove methylene blue from water.

2. Experimental

2.1. Starting chemicals

Glutaric anhydride ($C_5H_6O_3$), citric acid ($C_9H_{23}NO_3Si$), tetraethyl orthosilicate (TEOS), 3-(triethoxysilyl)propylamine, ferric nitrate ($Fe(NO_3)_3$), cobalt nitrate ($Co(NO_3)_2$), benzene-1,3,5-tricarboxylic acid (H_3BTC), copper nitrate trihydrate ($CuN_2O_6.3H_2O$), ethanol(C_2H_5OH), hydrochloric acid (HCl), methylene blue ($C_{16}H_{18}C_lN_3S$) and hydrogen peroxide, as the starting chemicals were purchased from Merck company and have been used without further purification.

2.2. Synthesis of $CoFe_2O_4@SiO_2$ nanocomposite and surface modification

CoFe2O4@SiO2 nanocomposite was synthesized via a Pechini sol-gel method, which has been reported elsewhere [31]:

1. TEOS solution was prepared by dissolving 60 mL of tetraethyl orthosilicate in a mixture of 10 mL of water and 50 mL of ethanol and adjusting its pH to 1.5 by dropwise addition of dilute HCl.
2. 21.03 mmol (6.12 g) of $Co(NO_3)_2.6H_2O$ and 42.08 mmol (17.0 g) of $Fe(NO_3)_3 \cdot 9H_2O$ were separately dissolved in water (15 mL) and transferred to a 250 mL two-necked flask and blended under reflux for 30 min; The resulting solution was added dropwise into TEOS solution and stirred vigorously for two h. The obtained liquid was transferred into a crystallizer

and left in the air for seven days at room temperature to achieve the expected alcogel.

3. The gel dried in an oven at 110 °C at 24 h, calcined at 400 °C for two h with a rate of 10 °C/min.

$CoFe_2O_4@SiO_2$ (1 gr) was dissolved in 50 mL of ethanol and treated by ultrasonic irradiation for 10 min to be dispersed. Then, 2 mL of 3-(triethoxysilyl)propylamine was added into the resulted solution under reflux for six h. The subsequent sediment was separated by centrifuge and dispersed in 30 mL of ethanol using ultrasonic for 10 min. Then, 26.33 mmol (3 g) of glutaric anhydride was added to this suspension and blended for three h at 40 °C. The precipitate was separated and washed with deionized water.

2.3. Synthesis of magnetic $CoFe_2O_4@SiO_2$/HKUST-1 nanocomposite

Copper nitrate trihydrate (25 mmol), H_3BTC (22.5 mmol) and modified $CoFe_2O_4@SiO_2$ (1 g) were added into 60 mL of water under vigorous stirring and refluxed for eight hours. The resulted precipitate separated and washed with water (3 × 20 mL), ethanol (2 × 10 mL) and dried under vacuum at 150 °C for ten h to achieve $CoFe_2O_4@SiO_2$/HKUST-1.

2.4. Methylene blue removal study

The following procedure performed removal experiments in aqueous solutions containing MB:

To study the effect of pH, five samples of methylene blue solution with conc. 5 mgL^{-1} were prepared and the pH of the solutions was adjusted to 3, 5, 7, 8 and 10, by addition of HCl (0.1 M) or NaOH (0.1 M). $CoFe_2O_4$@SiO_2/HKUST-1 (0.01 g) was added to the samples to initiate the reaction. The reaction vessels were fixed in the sonication bath center and irradiated by ultrasound for 60 min, while the temperature of the sonication bath was kept constant at room temperature.

The sonication process was stopped consecutive times and the sampling was performed to determine the residual dye concentration. After centrifugation, the samples were subjected to UV-Vis spectroscopic measurements. The amount of MB adsorbed via the as-synthesized compound at equilibrium (q_e mg/g) was calculated by Equation (1).

(1) $$q_e = (C_0 - C_e) \times \frac{V}{M}$$

Where C_0 and C_e(mg/L) are the initial and equilibrium MB concentration, respectively, V(L) is the volume of the dye solution, and M (g) is the mass of the adsorbent.

The effect of initial dye concentration and the effect of sorbent dosage on dye removal was studied in different concentrations of MB, 5, 10, 20 (5 mg L^{-1}) and 0.01, 0.02 and 0.03 g $CoFe_2O_4$@SiO_2/HKUST-1, respectively.

3. Characterization

The thermal behaviors of the samples were evaluated using a simulated thermal analyzer (STA, Pyris Diamond). The XRD patterns were obtained on an X-ray diffractometer (PANalytical, Philips, the Netherlands). The FTIR spectra were recorded on a spectrophotometer (Spectrum One, Perkin Elmer, Shelton, CT, USA). The SEM and TEM micrographs were acquired by an LEO SEM microscope (LEO 1455VP, Carl Zeiss Microscopy, Germany) and a Philips TEM microscope (CM20 FEG, Philips, the Netherlands). Vibrating sample magnetometer (VSM) used for the magnetic properties.

4. Results and discussion

4.1. X-Ray ray diffraction analysis

Figure 2 depicts the XRD patterns of the as-synthesized samples. The $CoFe_2O_4@SiO_2$ pattern contains $CoFe_2O_4$ and SiO_2 amorphous. This notion confirms matching with JSPDS, PDF#22-1086, and JSPDS, PDF#77-126, SiO_2. Diffraction patterns of the $CoFe_2O_4@SiO_2$/HKUST-1 sample consist of the $CoFe_2O_4@SiO_2$ diffraction peaks as well as those of the HKUST-1 compound (JCPDS: 1-276). The diffraction patterns of the sample were in good agreement with published literature reports [32-33]. The diffraction intensities of specific

peaks of $CoFe_2O_4@SiO_2$ dramatically decreased, implying that the existence of HKUST-1 leads to partial decomposition of the crystalline form of $CoFe_2O_4@SiO_2$ and probably decreasing to a SiO_2 amorphous phase.

4.2. FTIR analysis

In Figure 4 and Table 1, the characteristic IR absorptions of $CoFe_2O_4@SiO_2$ and $CoFe_2O_4@SiO_2$/HKUST-1 samples are summarized, confirming the formation of the mentioned compounds. Figure 4a shows that the two bands at 472 and 964 cm^{-1} can be attributed to the stretching of Si-O and Fe-O-Si bonds in $CoFe_2O_4@SiO_2$. The main peaks at 803 and 1080 cm^{-1} can be assigned to the Si-O-Si symmetric and asymmetric stretching and bending vibrations. The weak signatures observed at 580 cm^{-1} for the metal oxide (Co, Fe-O) reveal that the magnetite particles are linked by silicon oxide. It is not common to see peaks about 1640 cm^{-1} in similar compounds; mostly, the C=O stretching vibrations of amides are seen in this region. A weak intense peak at 2930 cm^{-1} possibly relates to the alkenes. Finally, broad and strong peaks centered at 3435 cm^{-1} suggest the presence of H-bonding in the compound. These results match entirely to previous similar work [34].

The chief peak at 522 cm^{-1} for $CoFe_2O_4@SiO_2$ is more intense relative to the similar one for $CoFe_2O_4@SiO_2$/HKUST-1, while they originate from Co, Fe-O

vibrations in both compounds and indicates more freedom of M-O vibrations for the first compound. The corresponding absorption is absent in $CoFe_2O_4$@SiO_2/HKUST-1 because of the overlapping of the Co, Fe-O vibrations with the silica peak at 1080 cm^{-1}. There are some medium bands at the frequencies 683-798 $cm^{-1,}$ ascribed as the C-H vibrations and possibly due to out-of-plane aromatic modes. The peak at 992 cm^{-1} may be aroused from the =C-H bending mode, common for alkenes. Some weak signals at 1119-1387 cm^{-1} are related to the -C-H stretching vibration of carboxylic acids or alkenes. The peak observed at 1615 cm^{-1} is assigned to C=C stretching band emanated from aromatic compounds. There are two medium peaks at 1453 and 1564 cm^{-1}, which could be given to C-C and C=C bonds and stem from in-ring aromatic stretching vibrations. Observation of two peaks at 1707 and 1900 cm^{-1} is due to the vibrations of C=C bonds and indicates the presence of BTC molecules. A peak of very weak intensity at 2553 cm^{-1} is attributed to carboxylic acids emanated from HKUST-1 MOF [35]. Two absorption peaks appearing at 3074 and 3117 cm^{-1} are due to the =C-H stretches of aromatic compounds. The strong peaks at 3405 cm^{-1} imply the presence of H–bonding. Thus, the FT-IR spectra confirm the fabrication of the $CoFe_2O_4$@SiO_2/HKUST-1 composite.

4.3 .Morphology observations

As depicted in figure 3, SEM and TEM measurements were performed to evaluate the morphology and particle distribution for $CoFe_2O_4@SiO_2$ and $CoFe_2O_4@SiO_2$/HKUST-1 samples. Figure 3a shows that the morphology of $CoFe_2O_4@SiO_2$ samples is semi-spherical and unevenly. The picture shows the agglomeration of particles; it may be due to covering particles via a silica matrix that affects the compound. As can be seen, in figure 3b, the morphology of the $CoFe_2O_4@SiO_2$/HKUST-1 sample is approximately octahedral with uniform dispersion. Therefore, HKUST-1 morphology is predominant in the general formation of the aimed composite. According to this, the morphology of $CoFe_2O_4@SiO_2$ is different from the final-synthesized compound, suggesting the success of the synthesis of $CoFe_2O_4@SiO_2$/HKUST-1 .

The compound morphology was further confirmed by TEM. Based on Figures 3-c and 3d, two different octahedral and rod-like shapes have been achieved in the compound morphology. In figure 3-c, relatively small semi-spherical $CoFe_2O_4@SiO_2$ particles and rod-like shape with length and width of 10 μm and 150 nm, respectively, that could be originated from HKUST-1, embedding together. Furthermore, figure 3-d demonstrates that $CoFe_2O_4@SiO_2$/HKUST-1 has symmetrical octahedral morphology and contains particles with a size of about 50±5 nm.

4.4. Specific surface area measurement

Nitrogen adsorption-desorption isotherm, the specific surface area and pore structures of $CoFe_2O_4@SiO_2$/HKUST-1 are shown in figure 5 and table 2. The nitrogen adsorption-desorption isotherm shows the type II isotherm and the dimension of the pores agreed that the $CoFe_2O_4@SiO_2$/HKUST-1 is mesoporous. The Brunauer–Emmett–Teller (BET) specific surface area for $CoFe_2O_4@SiO_2$/HKUST-1 composite is only 27 (m^2g^{-1}). Mean pore sizes, 10 (nm), and pore size distribution ($cm^3\ g^{-1}$), calculated by the Barrett-Joyner-Halenda (BJH). These low values may originate from SiO_2 particles inside the frame, leading to porosity becoming blocked. This result is good evidence for the successful synthesis of the $CoFe_2O_4@SiO_2$/HKUST-1 composite. Because in our published report [35], this composite's specific surface area value in the absence of SiO_2 was 982.05 (m^2g^{-1}).

4.5. Magnetic behavior

Figure 5. shows the hysteresis curves of $CoFe_2O_4@SiO_2$ and $CoFe_2O_4@SiO_2$/HKUST-1, which VSM has measured. The magnetic saturation, Ms, for $CoFe_2O_4@SiO_2$ and $CoFe_2O_4@SiO_2$/HKUST-1 is 0.17 and 0.10 emu/g, respectively, exhibiting a decrease of Ms addition of HKUST-1. The magnetization of compounds is affected by particle size, particle shape, and synthesis method, so that this result can be attributed to reduced particle size and changes in the

structure of the surface of the compounds. On the other hand, the coercive force, Hc, does not change after the combination of HKUST-1 and is less than 1000 A / m for both compounds, which indicates the soft magnetic behavior [36].

4.6. Simultaneous thermal analysis

Figure 1 depicts the STA profile for investigating the thermal stability and temperature effects on the $CoFe_2O_4$@SiO_2/HKUST-1 compound. The synthesized sample was calcinated at 400 °C as can be seen from the TG thermogram, representing the weight change of the sample as a function of furnace temperature. It should be noted that there are three stages for weight loss. At the first stage, minimum temperature T_i, slight weight loss of about 8 wt.% occurs between 100-200 °C, which is due to evaporation of absorbed water and solvents into the composite. The second and third weight loss, approximately 70% wt., occurs in the range of 200-400 ° C, probably due to the organic moiety decomposition. Based on the DTA curve, as the temperature increases at 200 and 350 °C, two exothermic changes occur. Following similar reports [32, 37], these changes are probably due to the weight loss of the as-synthesized compound and could be due to the mass transfer between the sample and the surrounding gas phase. After 400 ° C and continuing up to 600 °C, there is no significant weight loss, indicating the

stability of residue of $CoFe_2O_4@SiO_2$/HKUST-1, which can be used to determine the optimum temperature of the calcination.

4.7. Methylene blue removal on $CoFe_2O_4@SiO_2$/HKUST-1 sample

Methylene blue removal studies under various conditions such as different pH of solutions, initial concentration of dye, the dosage of the as-synthesized compound and varied composite components were performed to achieve optimum conditions (see table 3). The results are summarized in Table 5.

4.7.1. Influence of pH

pH is one of the critical factors in determining the ability to remove pollutants because it directly affects the surface properties of composites and the ionization of the dye molecules [38]. According to Table 4 and Figure 8, removal efficiency has increased by increasing the pH of methylene blue solution from 3 to 10 to more than 95%. Therefore, the overall process efficiency at basic pH is significantly higher than at acidic pH so, the optimum pH for $CoFe_2O_4@SiO_2/Cu_3(BTC)_2$ Equal to 10 is considered. In alkaline environments, the surface of the compound is covered by negative OH ions, and as a result of more interactions with positive

ions, the removal efficiency increases. The electrostatic attraction between the composite and methylene blue causes the substance to separate and the dye removed by the synthesized sample. On the other hand, the data showed that the amount of dye removal was not meaningfully different in the range of pH = 7-10; this could be due to the equilibrium between the positive charges of methylene blue dye and the negative charges on the composite surface, so for further experiments, a mild alkaline system with pH = 10 was used.

4.7.2. Influence of initial MB concentration

Figure 9 shows the effect of dye concentration on MB removal by $CoFe_2O_4@SiO_2$/HKUST-1. Base on table 5, MB removal efficiency at different initial dye concentrations containing 5, 15, 25 mg−1 and a constant dose of the .composite (0.01 g per 100 ml) was 60, 50, and 40, respectively

As the dye concentration increases, the decolorization efficiency decreases, which is probably since at high concentrations, the active sites of the compound are covered by positively charged dye molecules.

4.7.3. Influence of $CoFe_2O_4@SiO_2$/HKUST-1 dosage

Figure 10 shows the effect of the amount of $CoFe_2O_4@SiO_2$/HKUST-1 on MB removal. Removal efficiency at different as-prepared composite dosages containing 0.01, 0.02, and 0.03 (g/L) decreases from 60 to 57% .

When the value of $CoFe_2O_4@SiO_2$/HKUST-1reaches 0.01 and 0.02, the maximum removal occurs. That is, with increasing the active surface area of the composite, the extent of decolorization increases. Above this value does not affect the removal efficiency. As a result, 0.01 (g) of $CoFe_2O_4@SiO_2$/HKUST-1was selected as the optimum value.

4.7.4 Influence of different component of the adsorption system

Figure 11 and Table 4 show the removal results of MB in the presence of synthesized compounds and demonstrate that the removal efficiency (R%) of methylene blue by $CoFe_2O_4@SiO_2$ and $CoFe_2O_4@SiO_2$/HKUST-1 for 60 minutes at pH 10 is approximately 100 %. Besides, the R% values for pure H_2O_2, $CoFe_2O_4$ and HKUST-1 were 36, 75 and 95, respectively. Comparing dye removal values by different compounds shows that $CoFe_2O_4@SiO_2$ and $CoFe_2O_4@SiO_2$/HKUST-1 can be considered potent candidates for MB removal. Since MB has a positive surface charge, these findings could be due to electrostatic interactions between the positive charge of methylene blue and the negative charge of composite surfaces.

4.7.5 Adsorption isotherms

To clarify the interaction of methylene blue with adsorbent Langmuir and Freundlich isotherm was studying .

In Langmuir theory, the basic premise is that adsorption occurs at a specific homogeneous site inside the adsorbent. This means that when the dye molecules attach to a location on the adsorbent surface, the molecule can no longer be located there. There is no interaction between the adsorbed molecules, and this theory is described by Equation (3).

$$\frac{C_e}{q_e} = \frac{1}{K_L q_{max}} + \frac{C_e}{q_{max}} \quad (3)$$

Where q_e (mg/g) and C_e (mg/L) are the adsorption capacity and the equilibrium concentration of the dye in solution, respectively. q_{max} (mg/L) max is the maximum absorption capacity and $K_L(L/mg)$ is the Langmuir constant.

One of the basic features of the Langmuir isotherm is the determination of the adsorption capacity for the separation of contaminants, which is defined by the separation factor R_L and equation (4). Also, if $0 < R_L < 1$, the result is desirable. Besides, the Langmuir isotherm is linear and irreversible when $R_L = 1$ and $R_L = 0$, respectively.

(4) $$R_L = \frac{1}{(1 + K_L * C_0)}$$

In Equation 4, C_0 is the maximum initial concentration (mg/L) and the K_L parameter is the Langmuir equation.

Freundlich isotherm is obtained by assuming a heterogeneous surface with non-uniform distribution of adsorption heat on the surface. The Freundlich isotherm predicts that as the concentration of dye in the aqueous solution increases, the dye concentration on the adsorbent surface increases, and this isotherm is described by Equation (5).

(5) $$\mathrm{Ln}\, q_e = \mathrm{Ln}\, K_f + \mathrm{Ln}\, {}^{C_e}/_{n}$$

Where $q_e(\mathrm{mg/g})$ and $C_e\ (\mathrm{mg/L})$ are adsorption capacity and equilibrium concentration of methylene blue.

The values of K and n are Freundlich constants. K_f values and n are calculated from the slope and the width from the origin of the diagram of $\log q_e$ versus $\log q_e$.

In the Freundlich isotherm, if the value of n is between 1 and 10, the adsorption process is acceptable, and also, when the values of n are less than 1, physical adsorption occurs.

Based on the data in Table 6 and Figure 12, the Langmuir isotherm model with R^2 = 0.89 was selected as a suitable model for the methylene blue adsorption process on $CoFe_2O_4@SiO_2/Cu_3(BTC)_2$, which indicates the single adsorption layer of methylene blue on the adsorbent.

In the present experiment, values of $R_L = 0$ for adsorbent concentrations (20/30 mg /L) indicate that the isotherm is linear and irreversible, and $R_L = 1$ for adsorbent concentration (10 mg /L) indicates that the system is linear and undesirable. In other words, the combination of $CoFe_2O_4@SiO_2/Cu_3(BTC)_2$ is a suitable adsorbent for the removal of contaminants at high concentrations. In the Freundlich isotherm, values of n are less than one. Therefore, dye removal was performed by physical adsorption.

4.7.6 Adsorption kinetics

When adsorption occurs by penetration from inside the layer or boundary, kinetics most often follow the first order. Equation (6) is used for the quasi-first order model.

(6) $$\log(q_e - q_t) = \log q_e - \frac{K_1}{2.303} t$$

In Equation 6, q_t and q_e are the amount of adsorbed material on the adsorbent at time t and at equilibrium time (mg/g) and K_1 is the pseudo-first-order adsorption rate constant $(1/\min)$, respectively. $\mathrm{Log}(q_e - q_t)$ is plotted against time to determine the constant value k and the coefficient R^2.

Pseudo-second-order kinetics shows that chemical adsorption is a step-slowing process that controls surface adsorption processes, and equation (7) is used to describe it. In general, this model is exciting and valuable because research has shown that the kinetics of most adsorption systems at different concentrations of pollutants are well compatible with this system. Also, the adsorption capacity, the second-order velocity constant, and the initial adsorption rate can be determined from this equation without knowing any previous coefficient.

(7) $$t/q_t = 1/K_2\, q_e^2 + t/q_e$$

In Equation 7, $(g/(mg\ min))$ K_2 is a quasi-quadratic absorption rate constant. The graph of t/q_t versus t is used to obtain velocity parameters and proposes the results of this kinetic model with experimental data. The values $q_e$and K_2 are determined by calculating the slope and width from the origin of this graph.

The initial rate of adsorption rate $h_{0,2}$ $(mg/(g\ min))$ can be calculated based on equilibrium adsorption capacity using Equation (8).

(8) $$h_{0,2} = k_2 q_e^2$$

The kinetic model influences the diffusion to investigate that the diffusion mechanism is absorbed in the porous adsorption and the phase shift that the velocity controller has and describes according to Equation 9.

(9) $$q_t = K_{diff} t^{1/2} + I$$

K_{diff} is a constant rate of intra-particle penetration in terms of (mg/g.min$^{0.5}$) and I width from the origin in terms of (mg/g) and indicates the thickness of the

boundary layer that determines the increase or decrease of intra-particle penetration. The regression line q_t (R^2) versus $t^{1/2}$ slope gives the K_{diff} parameter. The results of methylene blue adsorption kinetics on $CoFe_2O_4@SiO_2$ /$Cu_3(BTC)^2$ are summarized in Table 7. The results of methylene blue adsorption kinetics on $CoFe_2O_4@SiO_2$ /$Cu_3(BTC)^2$ are summarized in Table 7. The results showed that following the data from the reaction kinetics is intraparticle diffusion <pseudo-first-order < pseudo-second-order. It was also found that the calculated q_e values correspond to the experimental q_e.

Hence, the pseudo-second-order kinetic model better shows the adsorption kinetics. The function of quadratic equations also suggests that the adsorption process depends on the adsorption concentration because the pseudo-second-order equation is generally based on the absorption capacity (see Figure 13). According to the values of $h_{0,2}$, the initial adsorption rate increases at higher dye concentrations.

The values of R^2 related to intraparticle diffusion are calculated and shown in Table (13). Due to the high regression coefficient close to 0.91, this system can follow this model. As can be seen in Figure (13), the graphs are linear. The linearity of the graph shows that this kinetics plays an indispensable role in the adsorption process by $CoFe_2O_4@SiO_2/Cu_3(BTC)_2$ but the model of intraparticle diffusion alone. The mechanism does not control the initial velocity of adsorption

and the mechanism of adsorption and diffusion of intra-particles is done simultaneously.

5. Conclusion

In this research, the $CoFe_2O_4@SiO_2$ core was modified by glutaric anhydride and 3-(triethoxysilyl)propylamine, based on the in situ self-assembly method was introduced into a solution containing copper acetate and 1,3,5-benzene tricarboxylic acid to fabricate the $CoFe_2O_4@SiO_2$/HKUST-1 magnetic metal-organic framework. It is a new organic-inorganic magnetic framework used for removing methylene blue, but further potential applications could be the subject of research .

The FT-IR spectra and XRD patterns confirmed that the prepared compound contains all of its constituent components. According to microscopic observations, there are two octahedral and rod-like shapes in the final powder, a mesoporous compound. The soft ferrimagnetic behavior of the sample was approved via the evaluation of magnetization curves.

$CoFe_2O_4@SiO_2$ and $CoFe_2O_4@SiO_2$/HKUST-1 remove methylene blue with 100% efficiency from aqueous media so that they can be considered as suitable decolorizing reagents in aqueous systems. As the amount of

$CoFe_2O_4$@SiO_2/HKUST-1 increases, the removal rate rises due to the increase in active sites, but the higher the initial dye concentration, the lower the decolorization efficiency.

References

[1] C. Sanchez, B. Julián, P. Belleville, M. Popall, Applications of hybrid organic-inorganic nanocomposites, J. Mater. Chem. (2005). https://doi.org/10.1039/b509097k.

[2] O.K. Farha, J.T. Hupp, Rational design, synthesis, purification, and activation of metal-organic framework materials, Acc. Chem. Res. (2010). https://doi.org/10.1021/ar1000617.

[3] H.C. Zhou, J.R. Long, O.M. Yaghi, Introduction to metal-organic frameworks, Chem. Rev. (2012). https://doi.org/10.1021/cr300014x.

[4] H.C.J. Zhou, S. Kitagawa, Metal-Organic Frameworks (MOFs), Chem. Soc. Rev. (2014). https://doi.org/10.1039/c4cs90059f.

[5] H. Furukawa, K.E. Cordova, M. O'Keeffe, O.M. Yaghi, The chemistry and applications of metal-organic frameworks, Science (80-.). (2013). https://doi.org/10.1126/science.1230444.

[6] R.J. Kuppler, D.J. Timmons, Q.R. Fang, J.R. Li, T.A. Makal, M.D. Young, D. Yuan, D. Zhao, W. Zhuang, H.C. Zhou, Potential applications of metal-

organic frameworks, Coord. Chem. Rev. (2009). https://doi.org/10.1016/j.ccr.2009.05.019.

[7] V. Russo, M. Hmoudah, F. Broccoli, M.R. Iesce, O.-S. Jung, M. Di Serio, Applications of Metal Organic Frameworks in Wastewater Treatment: A Review on Adsorption and Photodegradation, Front. Chem. Eng. (2020). https://doi.org/10.3389/fceng.2020.581487.

[8] A. Lajevardi, M. Hossaini Sadr, M. Tavakkoli Yaraki, A. Badiei, M. Armaghan, A pH-responsive and magnetic Fe_3O_4@silica@MIL-100(Fe)/β-CD nanocomposite as a drug nanocarrier: Loading and release study of cephalexin, New J. Chem. 42 (2018) 9690–9701. https://doi.org/10.1039/c8nj01375f.

[9] G. Wu, J. Ma, S. Li, J. Guan, B. Jiang, L. Wang, J. Li, X. Wang, L. Chen, Magnetic copper-based metal organic framework as an effective and recyclable adsorbent for removal of two fluoroquinolone antibiotics from aqueous solutions, J. Colloid Interface Sci. (2018). https://doi.org/10.1016/j.jcis.2018.05.105.

[10] Y. Xu, J. Jin, X. Li, Y. Han, H. Meng, T. Wang, X. Zhang, Fabrication of hybrid magnetic HKUST-1 and its highly efficient adsorption performance for Congo red dye, RSC Adv. (2015). https://doi.org/10.1039/c5ra00384a.

[11] C.H. Hendon, A. Walsh, Chemical principles underpinning the performance

of the metal-organic framework HKUST-1, Chem. Sci. (2015). https://doi.org/10.1039/c5sc01489a.

[12] L. Li, X.L. Liu, M. Gao, W. Hong, G.Z. Liu, L. Fan, B. Hu, Q.H. Xia, L. Liu, G.W. Song, Z.S. Xu, The adsorption on magnetic hybrid Fe_3O_4/HKUST-1/GO of methylene blue from water solution, J. Mater. Chem. A. (2014). https://doi.org/10.1039/c3ta14225f.

[13] A. Lajevardi, M. Hossaini Sadr, A. Badiei, M. Armaghan, Synthesis and characterization of Fe_3O_4@SiO_2@MIL-100(Fe) nanocomposite: A nanocarrier for loading and release of celecoxib, J. Mol. Liq. (2020). https://doi.org/10.1016/j.molliq.2020.112996.

[14] R. Ricco, L. Malfatti, M. Takahashi, A.J. Hill, P. Falcaro, Applications of magnetic metal-organic framework composites, J. Mater. Chem. A. (2013). https://doi.org/10.1039/c3ta13140h.

[15] Y.J. Ma, X.X. Jiang, Y.K. Lv, Recent Advances in Preparation and Applications of Magnetic Framework Composites, Chem. - An Asian J. (2019). https://doi.org/10.1002/asia.201901139.

[16] Q.L. Zhu, Q. Xu, Metal-organic framework composites, Chem. Soc. Rev. (2014). https://doi.org/10.1039/c3cs60472a.

[17] T. Dippong, O. Cadar, E.A. Levei, I. Bibicu, L. Diamandescu, C. Leostean, M. Lazar, G. Borodi, L. Barbu Tudoran, Structure and magnetic properties of

$CoFe_2O_4/SiO_2$ nanocomposites obtained by sol-gel and post annealing pathways, Ceram. Int. 43 (2017) 2113–2122. https://doi.org/10.1016/j.ceramint.2016.10.192.

[18] A. Casu, M.F. Casula, A. Corrias, A. Falqui, D. Loche, S. Marras, Magnetic and structural investigation of highly porous $CoFe_2O_4$-SiO_2 nanocomposite aerogels, J. Phys. Chem. C. (2007). https://doi.org/10.1021/jp0650230.

[19] L. Huang, M. He, B. Chen, B. Hu, A designable magnetic MOF composite and facile coordination-based post-synthetic strategy for the enhanced removal of Hg^{2+} from water, J. Mater. Chem. A. 3 (2015) 11587–11595. https://doi.org/10.1039/c5ta01484k.

[20] Y. Lu, B. Wang, Y. Yan, H. Liang, D. Wu, Silica Protection–Sacrifice Functionalization of Magnetic Graphene with a Metal–Organic Framework (ZIF-8) to Provide a Solid-Phase Extraction Composite for Recognization of Phthalate Easers from Human Plasma Samples, Chromatographia. (2019). https://doi.org/10.1007/s10337-018-3673-3.

[21] H. Su, Y. Lin, Z. Wang, Y.L.E. Wong, X. Chen, T.W.D. Chan, Magnetic metal–organic framework–titanium dioxide nanocomposite as adsorbent in the magnetic solid-phase extraction of fungicides from environmental water samples, J. Chromatogr. A. (2016). https://doi.org/10.1016/j.chroma.2016.08.066.

[22] R. Wo, Q.L. Li, C. Zhu, Y. Zhang, G.F. Qiao, K.Y. Lei, P. Du, W. Jiang, Preparation and Characterization of Functionalized Metal-Organic Frameworks with Core/Shell Magnetic Particles (Fe_3O_4@SiO_2@MOFs) for Removal of Congo Red and Methylene Blue from Water Solution, J. Chem. Eng. Data. 64 (2019) 2455–2463. https://doi.org/10.1021/acs.jced.8b01251.

[23] R. Zhang, Z. Wang, Z. Zhou, D. Li, T. Wang, P. Su, Y. Yang, Highly Effective Removal of Pharmaceutical Compounds from Aqueous Solution by Magnetic Zr-based MOFs Composites, Ind. Eng. Chem. Res. (2019). https://doi.org/10.1021/acs.iecr.8b05244.

[24] F. Müller, Sustainable Development Goals (SDGs), Peripher. – Polit. • Ökonomie • Kult. (2015). https://doi.org/10.3224/peripherie.v35i140.23001.

[25] J. Liu, V. Hull, H.C.J. Godfray, D. Tilman, P. Gleick, H. Hoff, C. Pahl-Wostl, Z. Xu, M.G. Chung, J. Sun, S. Li, Nexus approach to global sustainable development, Nat. Sustain. (2018). https://doi.org/10.1038/s41893-018-0135-8.

[26] D. Moreno-Mateos, A. Alberdi, E. Morriën, W.H. van der Putten, A. Rodríguez-Uña, D. Montoya, The long-term restoration of ecosystem complexity, Nat. Ecol. Evol. (2020). https://doi.org/10.1038/s41559-020-1154-1.

[27] S.G. Al-Kindi, R.D. Brook, S. Biswal, S. Rajagopalan, Environmental

determinants of cardiovascular disease: lessons learned from air pollution, Nat. Rev. Cardiol. (2020). https://doi.org/10.1038/s41569-020-0371-2.

[28] T. Robinson, G. McMullan, R. Marchant, P. Nigam, Remediation of dyes in textile effluent: A critical review on current treatment technologies with a proposed alternative, Bioresour. Technol. (2001). https://doi.org/10.1016/S0960-8524(00)00080-8.

[29] A. Lajevardi, M. Tavakkoli Yaraki, A. Masjedi, A. Nouri, M. Hossaini Sadr, Green synthesis of MOF@Ag nanocomposites for catalytic reduction of methylene blue, J. Mol. Liq. (2019). https://doi.org/10.1016/j.molliq.2018.12.002.

[30] Q. Liu, H. Yu, F. Zeng, X. Li, J. Sun, C. Li, H. Lin, Z. Su, HKUST-1 modified ultrastability cellulose/chitosan composite aerogel for highly efficient removal of methylene blue, Carbohydr. Polym. (2020) 117402. https://doi.org/10.1016/j.carbpol.2020.117402.

[31] M. Heydari, M. Gharagozlou, M. Ghahari, S. Naghibi, $NiFe_2O_4@SiO_2@Cu_3(BTC)_2$ nanocomposite as a magnetic metal-organic framework, Appl. Organomet. Chem. (2020). https://doi.org/10.1002/aoc.5994.

[32] M. Gharagozlou, Influence of calcination temperature on structural and magnetic properties of nanocomposites formed by Co-ferrite dispersed in sol-

gel silica matrix using tetrakis(2-hydroxyethyl) orthosilicate as a precursor, Chem. Cent. J. (2011). https://doi.org/10.1186/1752-153X-5-19.

[33] K. Schlichte, T. Kratzke, S. Kaskel, Improved synthesis, thermal stability and catalytic properties of the metal-organic framework compound $Cu_3(BTC)_2$, Microporous Mesoporous Mater. (2004). https://doi.org/10.1016/j.micromeso.2003.12.027.

[34] L. Huang, M. He, B. Chen, B. Hu, A designable magnetic MOF composite and facile coordination-based post-synthetic strategy for the enhanced removal of Hg^{2+} from water, J. Mater. Chem. A. (2015). https://doi.org/10.1039/c5ta01484k.

[35] T. Saemian, M. Gharagozlou, M. Hossaini Sadr, S. Naghibi, Synthesis of $CoFe_2O_4$@Cu_3 $(BTC)_2$ nanocomposite as a magnetic metal-organic framework, Polyhedron. 174 (2019). https://doi.org/10.1016/j.poly.2019.114163.

[36] C. Fei, Y. Zhang, Z. Yang, Y. Liu, R. Xiong, J. Shi, X. Ruan, Synthesis and magnetic properties of hard magnetic ($CoFe_2O_4$)-soft magnetic (Fe_3O_4) nanocomposite ceramics by SPS technology, J. Magn. Magn. Mater. (2011). https://doi.org/10.1016/j.jmmm.2011.02.014.

[37] X.H. Huang, Z.H. Chen, $CoFe_2O_4$ nanoparticles hosted in silica xerogels, Scr. Mater. (2006). https://doi.org/10.1016/j.scriptamat.2005.09.043.

[38] T. Saemian, M. Gharagozlou, M. Hossaini Sadr, S. Naghibi, A Comparative Study on the Pollutant Removal Efficiency of $CoFe_2O_4$@HKUST-1 MOF and $CoFe_2O_4$ Nanoparticles, J. Inorg. Organomet. Polym. Mater. (2019). https://doi.org/10.1007/s10904-019-01406-7.

Acknowledgment

We thank Azarbaijan Shahid Madani University for its financial support.

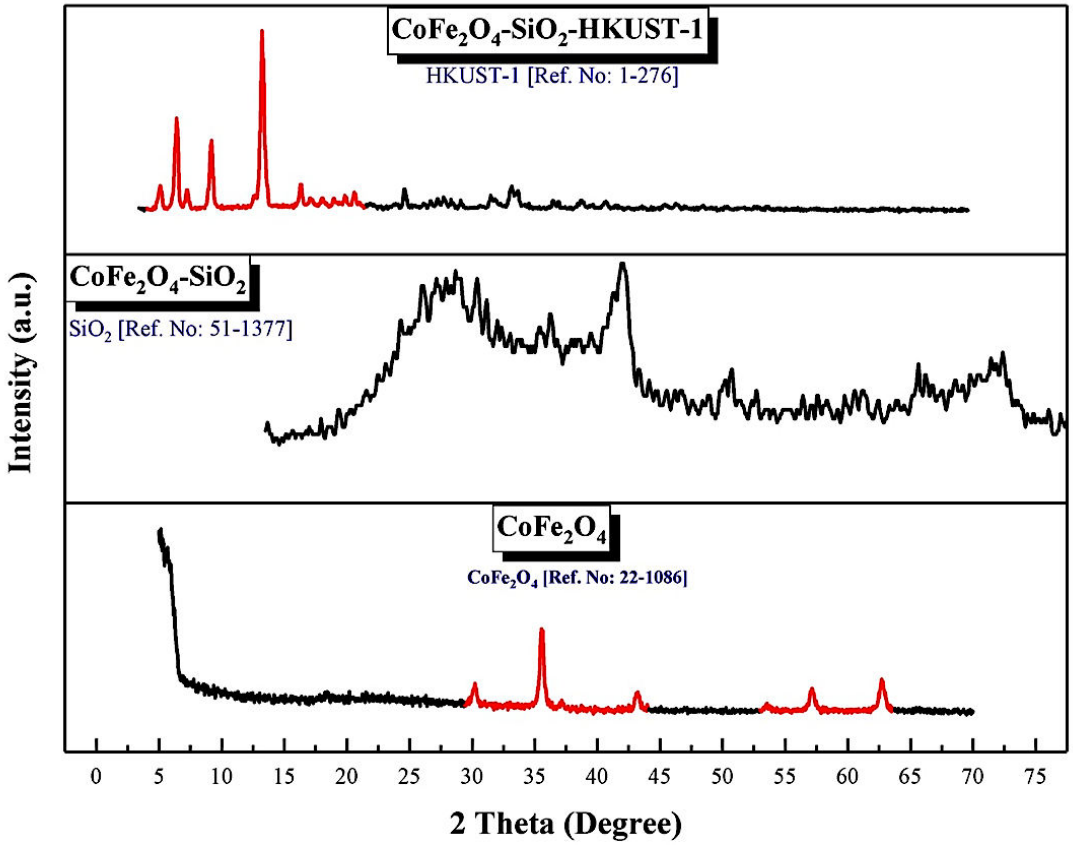

Fig. 1. The XRD patterns of $CoFe_2O_4@SiO_2$ and $CoFe_2O_4@SiO_2$/HKUST-1 compounds.

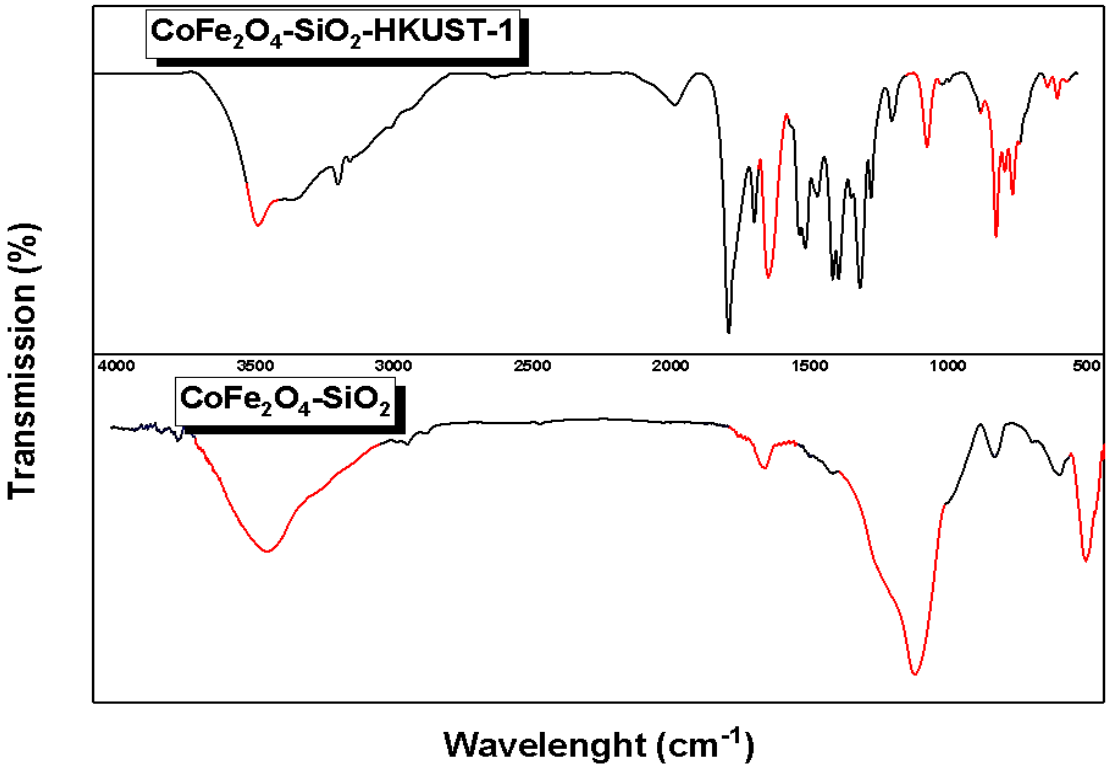

Fig. 2. FTIR spectra of $CoFe_2O_4@SiO_2$ and $CoFe_2O_4@SiO_2$/HKUST-1 compounds.

Table 1. Frequencies and assignments of FTIR bands in $CoFe_2O_4@SiO_2$ and $CoFe_2O_4@SiO_2$/HKUST-1 samples

Related compound	Function group	bond	Frequency (cm^{-1})
$CoFe_2O_4$-SiO_2		Si-O-Si symmetric	473 (m)
		M-O & Fe, Co-O	581 (m)
		Fe-O-Si	804 (m)

		SiO	965 (m)
		Si-O-Si asymmetric	1081 (b, s)
	Amides	υ C=O	1638 (m)
	Atmospheric CO_2	-	2334 (w)
	alkanes	υ –C–H	2930 (w)
	alcohols, phenols	δ H–bonded	3436 (b, s)
$CoFe_2O_4$@SiO_2/HKUST-1		M-O-Si	523 (w)
	aromatics	C–H "oop" (out-of-plane)	684-799 (sh, m)
	alkenes	δ =C–H	992 (m)
	alcohols, carboxylic acids, alkenes	υ C–O	1111-1388 (w)
	Aromatic compounds	υ C–C (in–ring)	1453 (b, m)
		υ C=O (in–ring)	1565 (m)
		υ C=C	1615 (sh, w)
	BTC	υ C=O stretch	1708- 901 (n, s)

	carboxylic acids	υ O–H stretch	2553 (w)
	aromatics	υ =C–H	3074-3118 (w)
	alcohols, phenols	δ H–bonded	3406 (b, s)
m=medium, w=weak, s=strong, n=narrow, b=broad, sh=sharp, υ = stretching vibration, and δ = bending vibration			

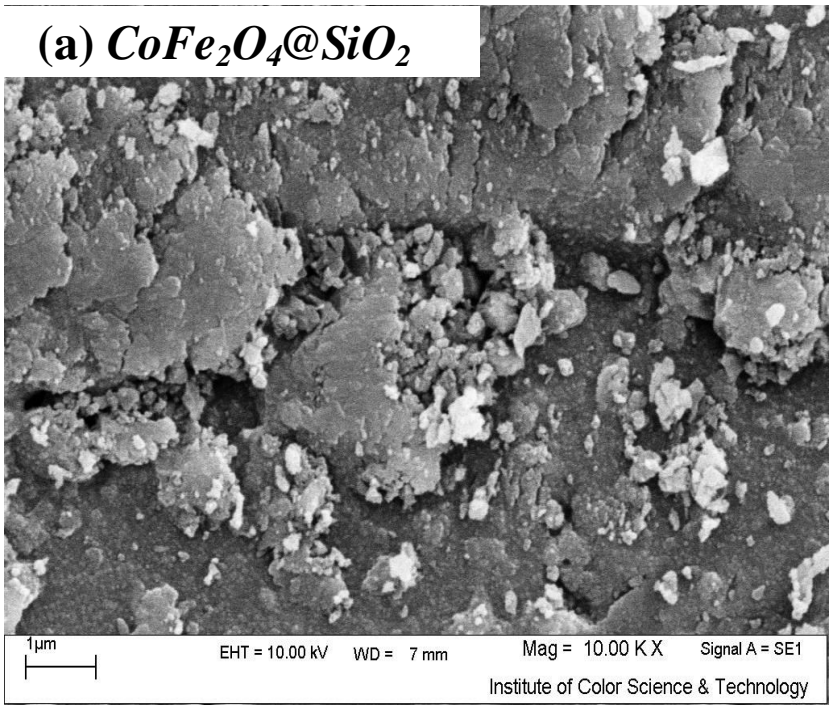

(b) *$CoFe_2O_4$@SiO_2/HKUST-1*

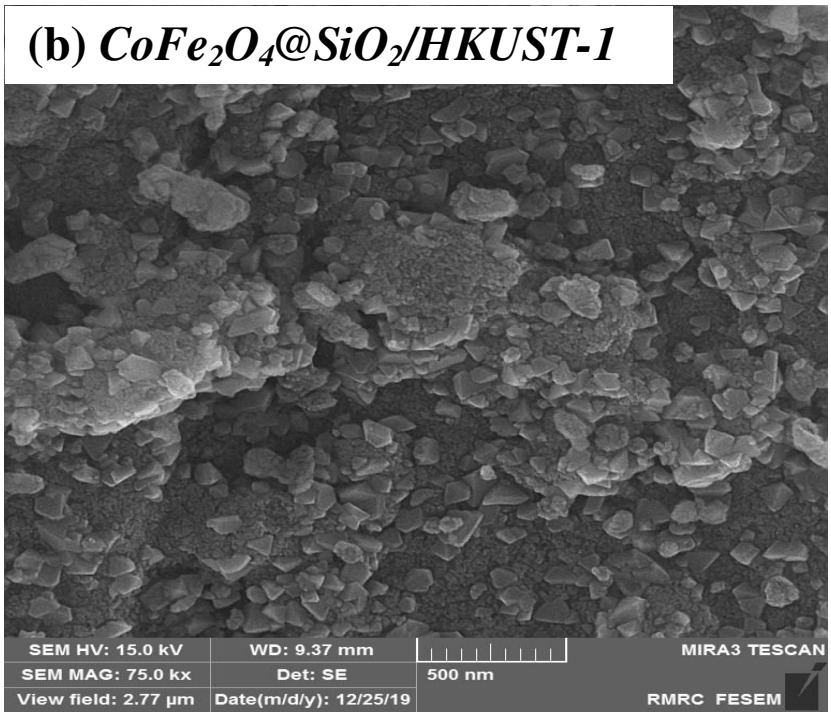

(c) $CoFe_2O_4$@SiO_2/HKUST-1

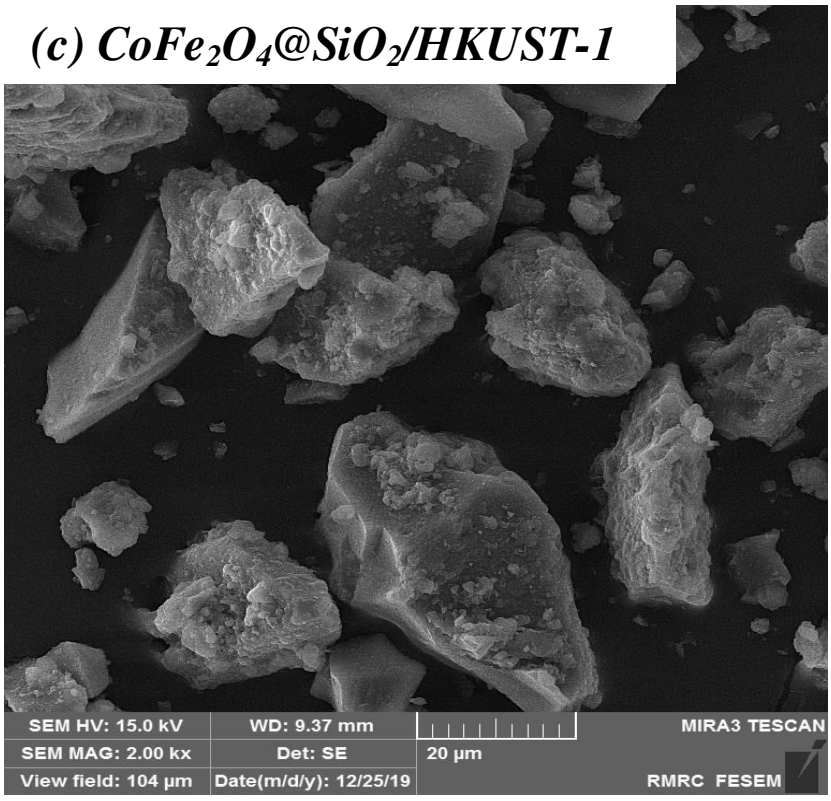

Fig. 3. SEM images of as-synthesized compounds; (a) $CoFe_2O_4@SiO_2$, (b, c) $CoFe_2O_4@SiO_2$/HKUST-1

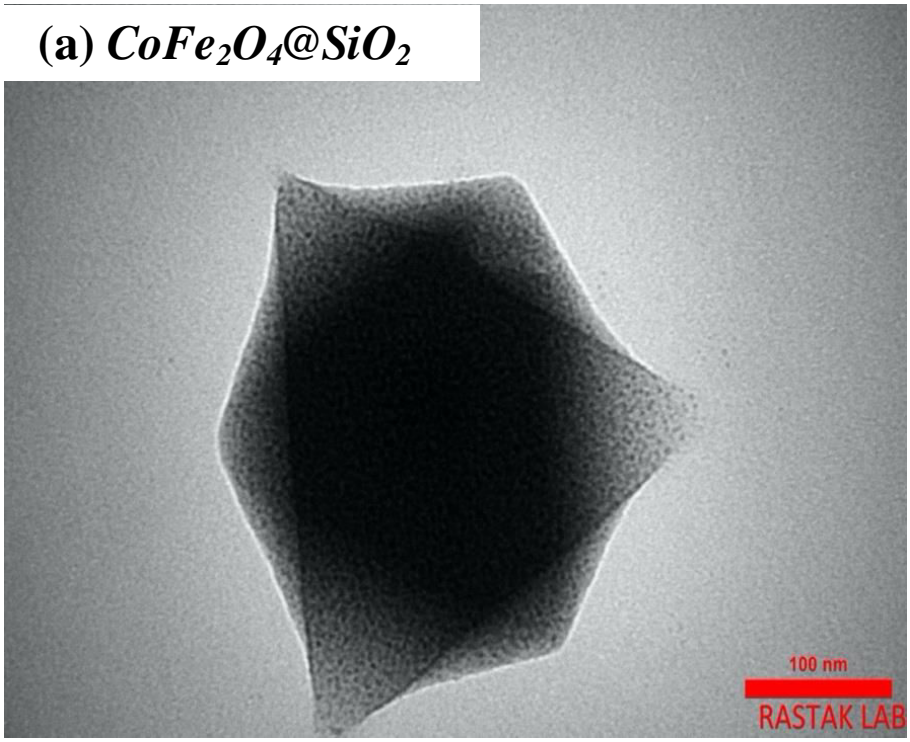

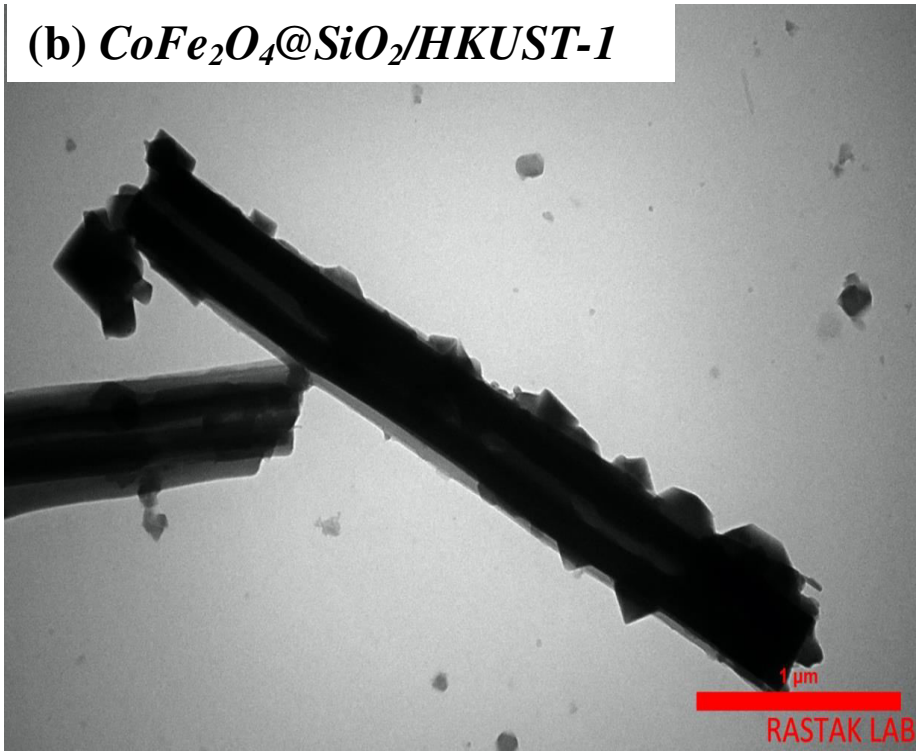

Fig. 4. TEM images of as-synthesized compounds; $CoFe_2O_4$@SiO_2/HKUST-1

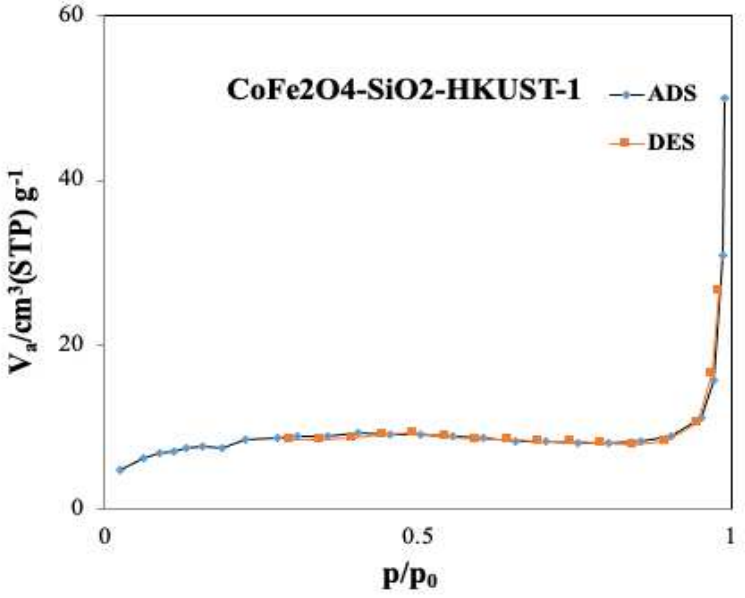

Fig. 5. Nitrogen adsorption-desorption isotherms graphs of $CoFe_2O_4$@SiO_2/HKUST-1 compound

Table 2. Numeral results of the Ads-Des and BET graphs of the as-synthesized $CoFe_2O_4$@SiO_2/HKUST-1 sample

Sample	BET			BJH		Ads-Des
	$a_{s,BET}$ [$m^2\ g^{-1}$]	d_{BET} [nm]	V_{BET} [$cm^3\ g^{-1}$]	$r_{p,peak}$ [nm]	a_p [$m^2\ g^{-1}$]	microporous or mesoporous
$CoFe_2O_4$@SiO_2/HKUST-1	27	10	0.07	1.21	7	**Non-porous**

Note: $a_{S,\,BET}$: BET specific surface area, d_{BET}: mean pore diameter, V_{BET}: total pore volume, $r_{p,\,peak}$: pore radius, a_P: BJH specific surface area. Abbreviations: BET, Brunauer–Emmett–Teller; BJH, Barrett–Joyner–Halenda.

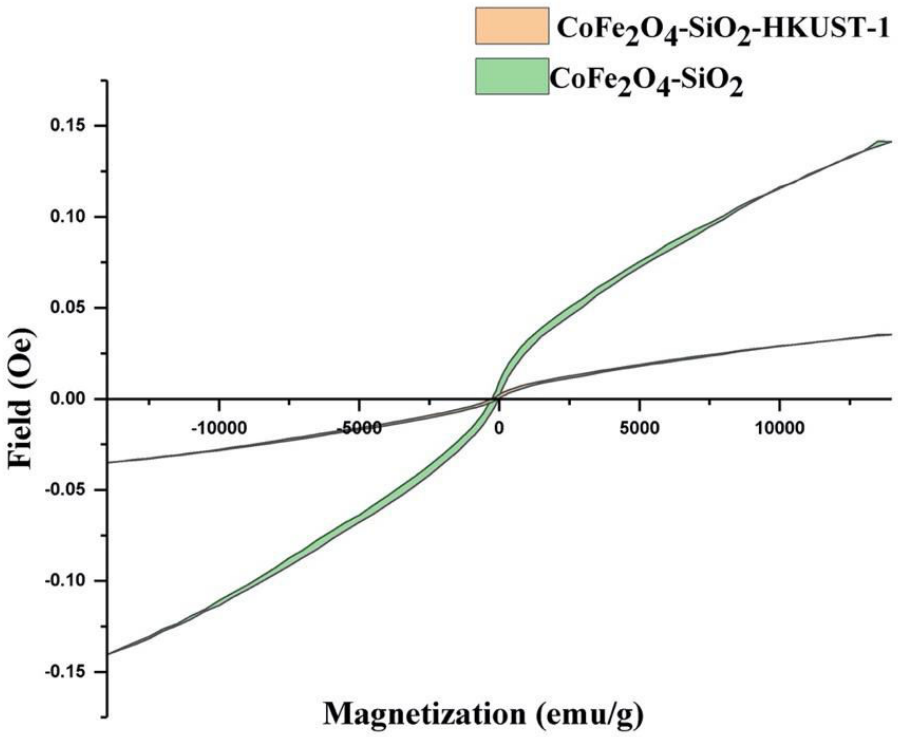

Fig. 6. The hysteresis curves of the compounds $CoFe_2O_4@SiO_2$ and $CoFe_2O_4@SiO_2$/HKUST-1 compounds

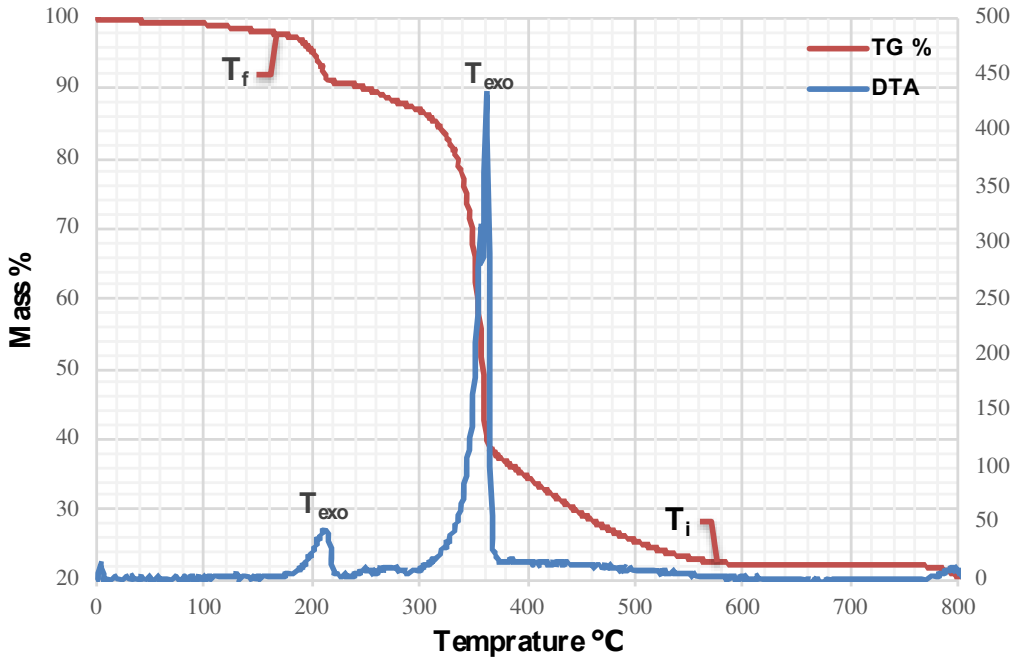

Fig. 7. TGA and DTA profiles of the $CoFe_2O_4$@SiO_2/HKUST-1 compound

Table 3. Investigation of various empirical factors for methylene blue degradation by $CoFe_2O_4$@SiO_2/HKUST-1 composite

Factors	**Unit**	**Levels**		
		Low (-1)	**Central (0)**	**High (+1)**
Methylene blue concentration	$mg\ L^{-1}$	5	15	25
$CoFe_2O_4$@SiO_2/HKUST-1dosage	g	0.01	0.02	0.03
pH	-	3	7	10

Table 4. The effect of pH on methylene blue degradation by $CoFe_2O_4@SiO_2$/HKUST-1; MB concentration (5 mgL^{-1}); as-prepared compound dosage (0.01 g)

Sample	**Adsorbent concentration (g)**	**pH**	**R (%)**
$CoFe_2O_4@SiO_2$/HKUST-1	0.01	3	7
		5	22
		neutral	90
		8	95
		10	≈ 100

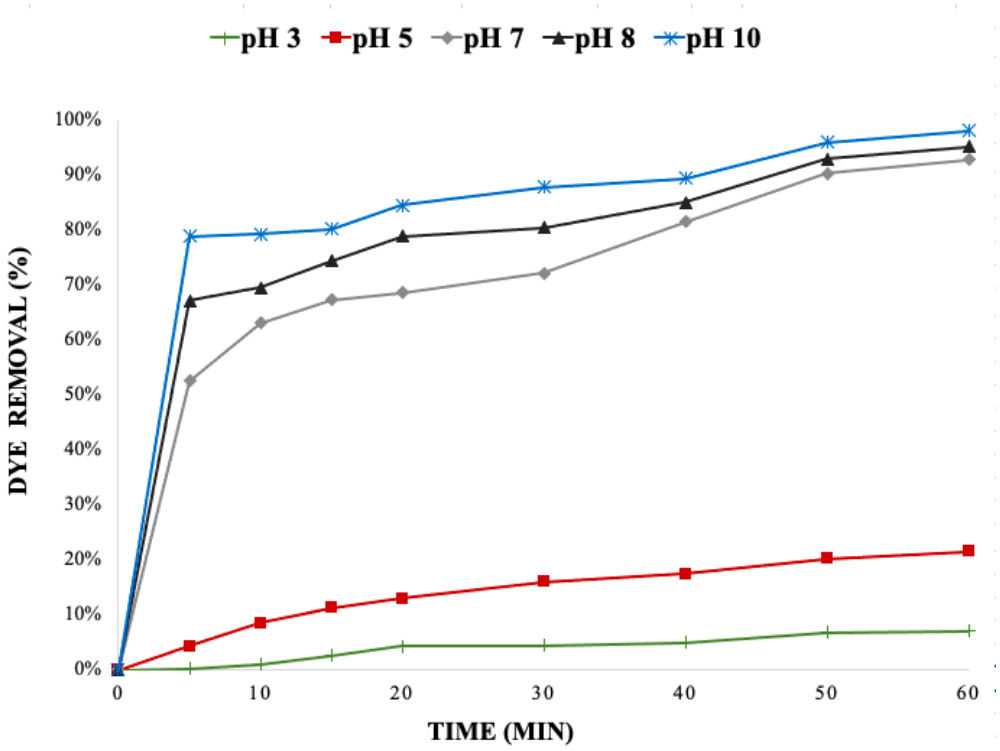

Fig. 8. The effect of variation of pH on methylene blue degradation by $CoFe_2O_4@SiO_2$/HKUST-1; MB concentration (5 mgL^{-1}); as-prepared composite dosage (0.01 g)

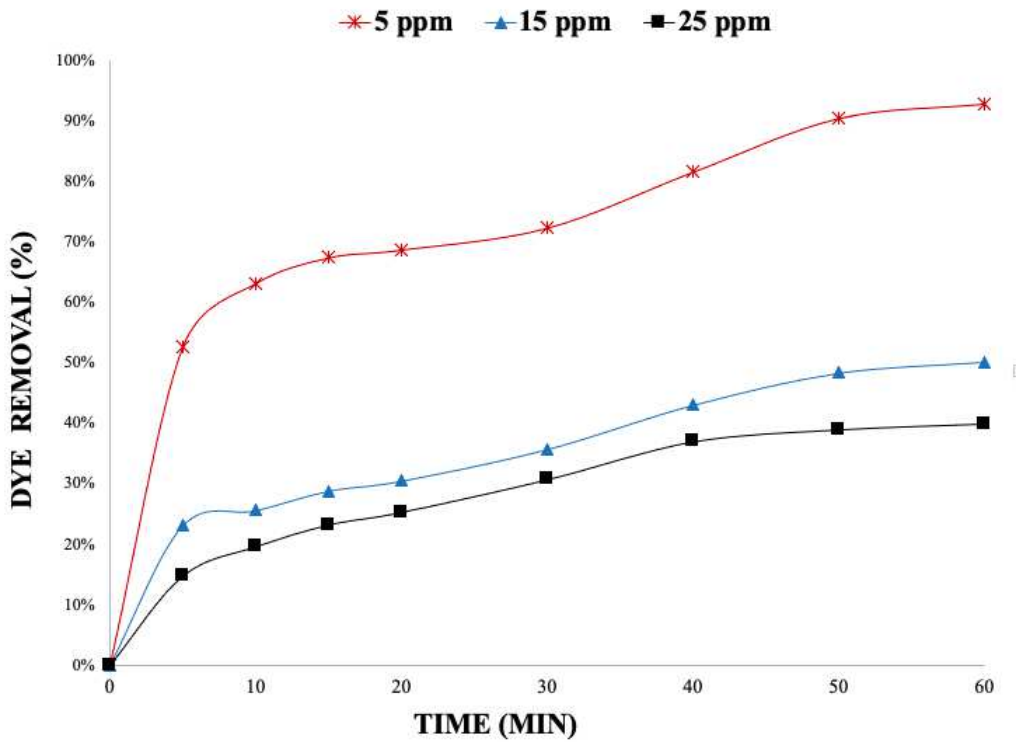

Fig. 9. The effect of dye concentration for methylene blue degradation by $CoFe_2O_4@SiO_2$/HKUST-1 composite; MB concentration (5, 15 and 25 mgL^{-1}); as-prepared composite dosage (0.01 g)

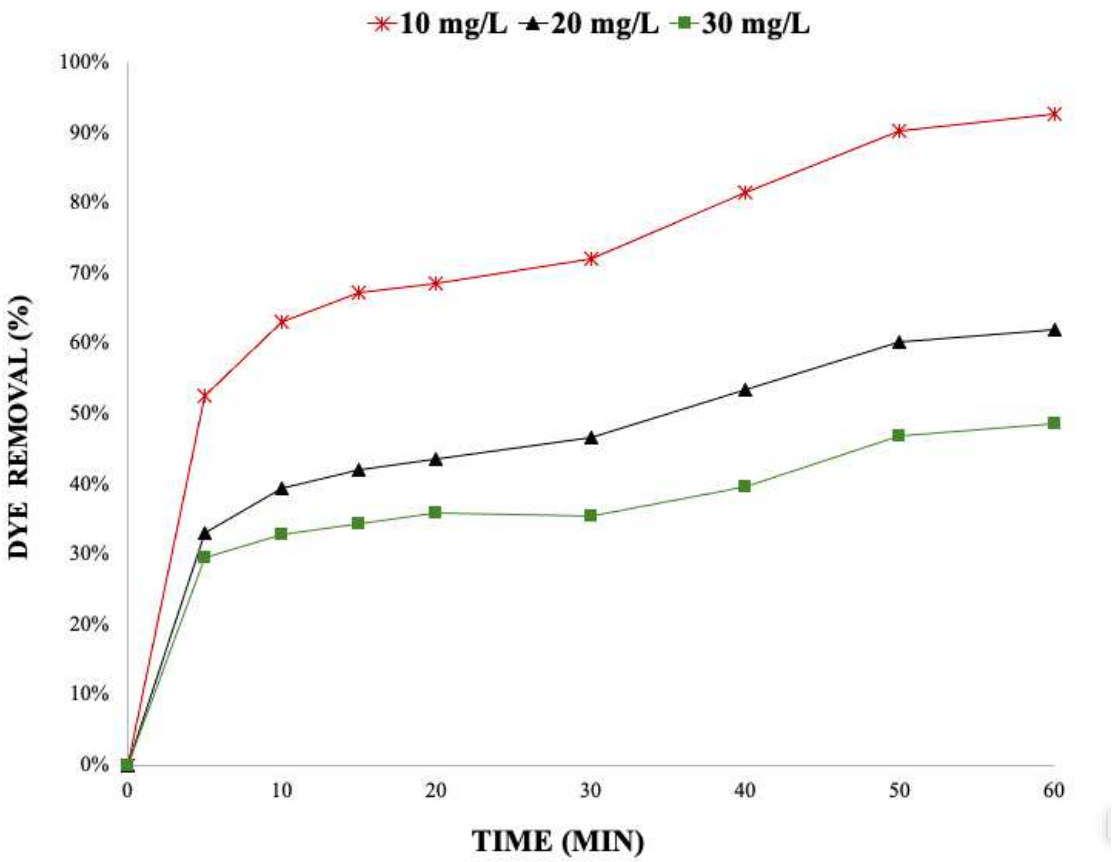

Fig. 10. The effect of $CoFe_2O_4@SiO_2$/HKUST-1 dosage for methylene blue degradation; MB concentration (5 mgL^{-1}); as-prepared composite dosage (0.01, 0.02 and 0.03 g)

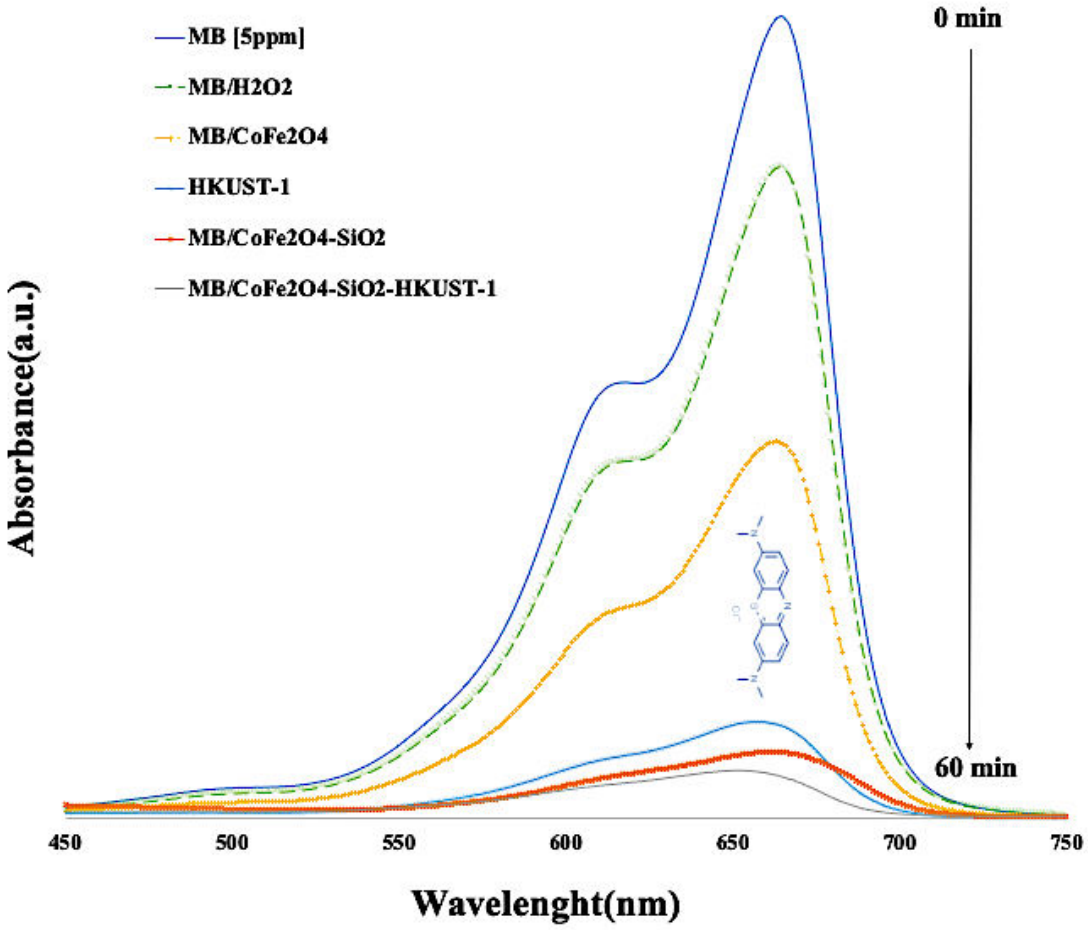

Fig. 11. The variation of UV–Visible absorption spectra for methylene blue degradation in the presence of different compound; H_2O_2, $CoFe_2O_4$, HKUST-1, $CoFe_2O_4@SiO_2$, and $CoFe_2O_4@SiO_2$/HKUST-1, on the optimum conditions; pH = 10, MB concentration = (5 mgL^{-1}), compounds dosage (0.01 g)

Table 5. The effects of initial dye concentration, as-prepared compound dosage parameters and different components of the composite for methylene blue degradation on the optimum conditions

Samples	Dye concentration (mg/L)	Compound dosage (g)	pH	R (%)	Absorption capacity (mg/g)
$CoFe_2O_4@SiO_2$/HKUST-1	25	0.01	neutral	40	49.29
	15			50	
	5			60	
		0.02		58	
		0.03		57	
H_2O_2		0.01	10	36	18.23
$CoFe_2O_4$				75	37.65
HKUST				95	47.32
$CoFe_2O_4@SiO_2$				> 95	49.50

Table 6. Langmuir and Freundlich model constants and R^2 values for methylene blue adsorption on $CoFe_2O_4@SiO_2/Cu_3(BTC)_2$

Dye	Adsorption Conc. (mg/L)	Langmuir model				Freundlich model		
		$q_L(mg\ g^{-1})$	$K_L(mg\ g^{-1})$	R^2	R_L	$K_F(mg\ q^{-1})$	$n(g\ L^{-1})$	R^2
Methylene blue	10	47.68	0.2×10^{-1}	0.88	1	8×10^{-1}	-2.08	0.52
	20	17.94	8.8×10^{-1}	0.89	0	7.3×10^{-1}	-4.23	0.75
	30	12.82	12.2×10^{-1}	0.70	0	7.1×10^{-1}	-6	0.83

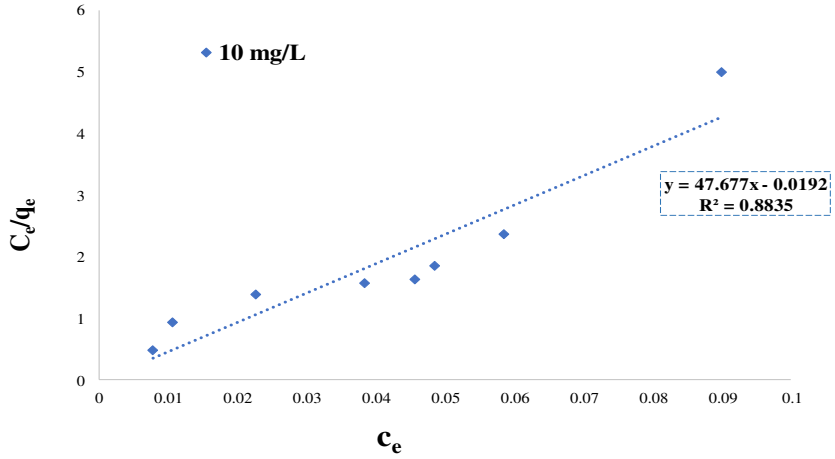
10 mg/L
y = 47.677x - 0.0192
R² = 0.8835
Ce/qe
Ce

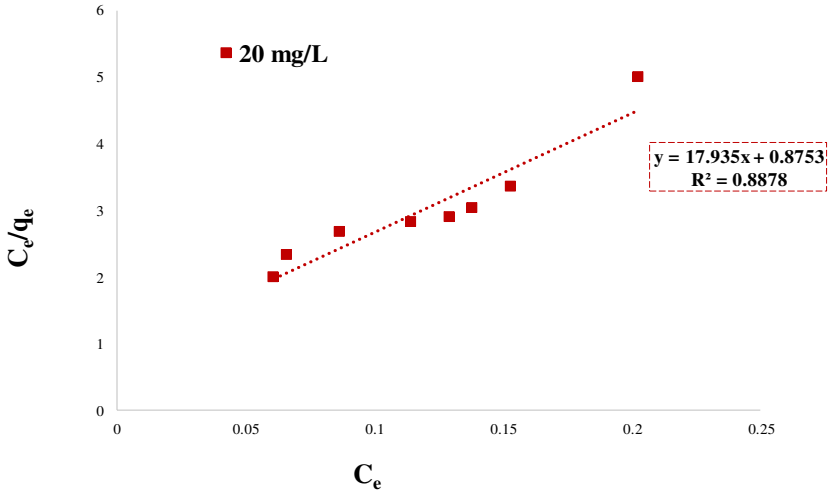
20 mg/L
y = 17.935x + 0.8753
R² = 0.8878
Ce/qe
Ce

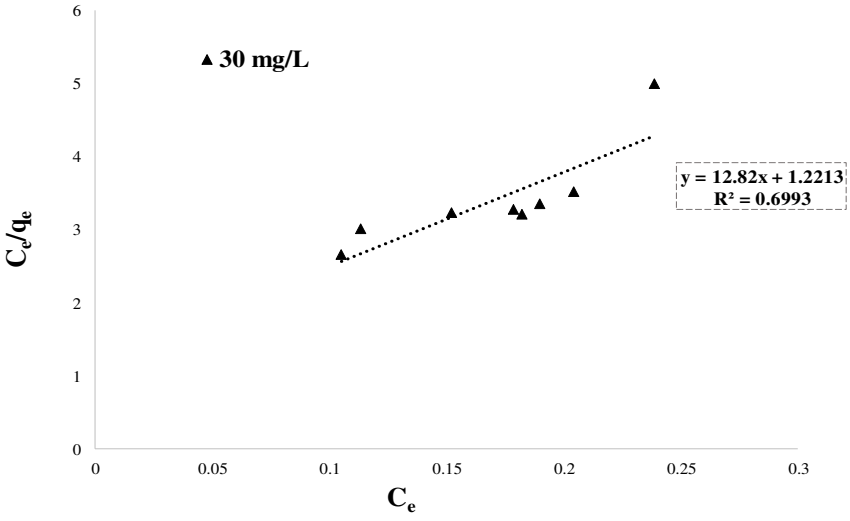
30 mg/L
y = 12.82x + 1.2213
R² = 0.6993
Ce/qe
Ce

Fig. 12. Langmuir model for the adsorption of methylene blue on $CoFe_2O_4@SiO_2/Cu_3(BTC)_2$

Table 7. Kinetic parameters and R^2 of pseudo-first and second-order adsorption models and intraparticle diffusion for methylene blue adsorption

Dye	Adsorption Conc. (mg/L)	$q_{e,exp}$	First-order-kinetic			Second-order-kinetic				Interparticle diffusion		
			K_1	$q_{e,Cal}$	R^2	K_2	$q_{e,Cal}$	R^2	$h_{0,2}$	K_p	I	R^2
Methylene blue	10	4.40	6×10^{-2}	35.15	0.88	4×10^{-3}	47/85	0.96	9.65	7.1×10^{-1}	0.99	0.87
	20	7.20	6×10^{-2}	73.04	0.90	7×10^{-4}	80.00	0.96	4.60	1.1×10^{-1}	0.56	0.91
	30	9.80	7×10^{-2}	11.14	0.95	8×10^{-4}	64.12	0.97	1.09	8×10^{-1}	0.34	0.84

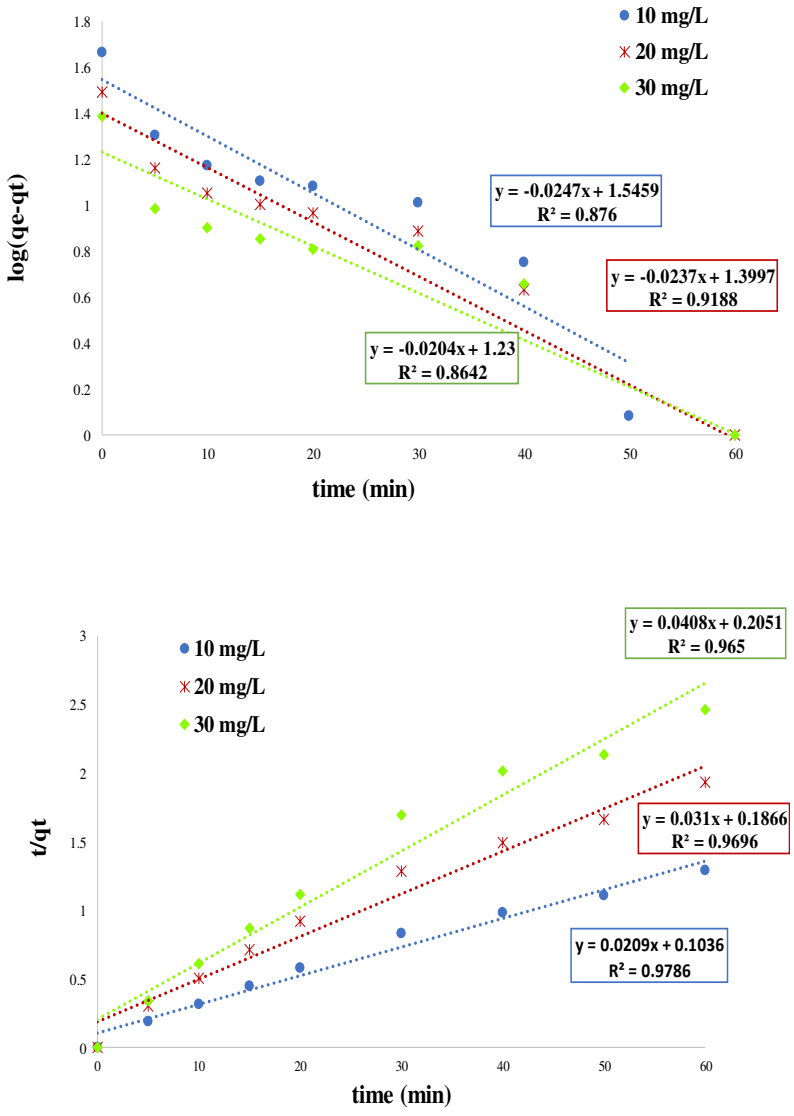

Fig. 13. The first and second quasi-first order kinetics models related to the adsorption of methylene blue on $CoFe_2O_4$@SiO_2 /HKUST-1

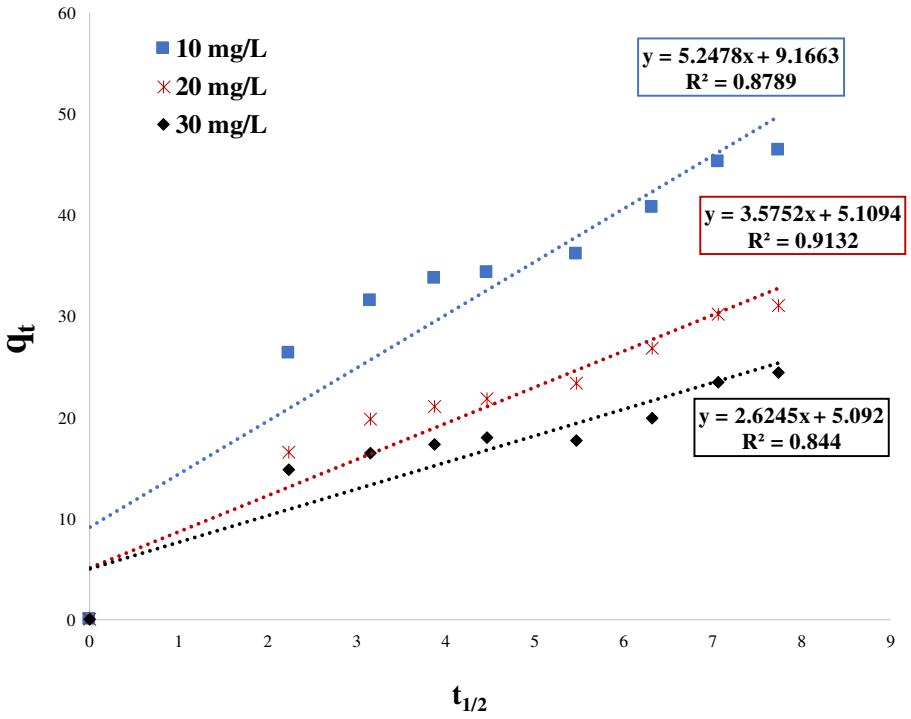

Fig. 14. Intraparticle diffusion diagrams related to methylene blue adsorption on $CoFe_2O_4@SiO_2$/HKUST-1

Highlight

✓ The three-metallic magnetic metal-organic framework , $CoFe_2O_4@SiO_2$/HKUST-1, was synthesized based on the in situ self-assembly technique

✓ $CoFe_2O_4@SiO_2$ and HKUST-1 were identified using XRD patterns

- ✓ TEM images of $CoFe_2O_4@SiO_2$/HKUST-1 contain two types of octahedral and rod-like morphologies
- ✓ $CoFe_2O_4@SiO_2$ and $CoFe_2O_4@SiO_2$/HKUST-1 are suitable materials for the removal of methylene blue in aqueous solutions

Supplementary Files

This is a list of supplementary files associated with this preprint. Click to download.

- GraphicalAbstractPictogramforreview.pdf